Solid Freeform Fabrication 2023: Proceedings of the 34th Annual International Solid Freeform Fabrication Symposium – An Additive Manufacturing Conference
Reviewed Paper

CONTROLLING CHEMICAL COMPOSITION CHANGES IN LASER POWDER BED FUSION OF ALSI10MG

Bochuan.Liu*[1], Gregory J. Gibbons[1]

[1]Warwick Manufacturing Group, University of Warwick, CV4 7AL, United Kingdom

*Corresponding author: Bochuan.Liu@warwick.ac.uk

ABSTRACT

Due to the large energy input during the laser powder bed fusion process, some elements of metal alloy will reach vaporisation temperature. Significant differences between the volatility of various elements in the alloy may change the chemical composition after manufacturing. This study used this preferential evaporation effect to control the final composition to a targeted value, potentially for alloy and component tracing. Different laser process parameter sets were studied, and the mechanical properties changes associated with various compositions were investigated.

Keywords: Laser Powder Bed Fusion (L-PBF), Preferential Evaporation, Chemical Composition, AlSi10Mg, Tensile Properties

1. INTRODUCTION

Additive manufacturing (AM) processes are an emerging technology that allows the fabrication of geometrically complicated components through the layer-by-layer building method [1]. One popular AM process, laser powder bed fusion (L-PBF) offers a novel route to manufacturing metal components for a variety of industries, such as aerospace, automotive, medical and defence. In the L-PBF process, thin layers of powder are deposited onto a build platform by a recoater, and a focused laser beam is used to consolidate the powder (through welding). When one layer is finished, a new layer of powder is applied, and the process is repeated until a 3D part is fabricated [2]. During the L-PBF process, a high temperature melting pool is introduced, and can cause substantial vaporisation of various volatile elements such as Lithium, Magnesium, Aluminium and Zinc [3]. When laser contacts the metal powder, these elements' high vapour pressure and low boiling temperature lead to their vaporisation [4]. These evaporative losses of the elements depend heavily on the maximum temperature inside the melting pool and the temperature-dependent vapour pressure of the constitutive elements [5], therefore, laser scanning parameters, which result in various laser energy densities, are essential factors in such cases [6,7].

When there is a significant difference between the boiling temperature of various elements in the metal alloy, the selective vaporisation of volatile elements may result in changes in the overall chemical composition. This observation has been documented during the L-PBF process of various aluminium-containing alloys, such as titanium aluminides [7-11] and Ti6Al4V [12].

Under certain laser scanning parameter sets, the loss of Al can reach up to 8 at.% (atomic ratio) [11].

In non-aluminium containing alloys, similar selective evaporation is also observed, including the elemental loss of chromium [13] in L-PBF of Inconel 718, and nickel [14] in NiTi alloys.

In this paper, AlSi10Mg was studied for possible selective evaporation effect. Main laser scanning parameters, such as laser power, scanning speed and hatch distance were modified to offer different energy densities; and the chemical composition changes and fabricated parts' quality were investigated.

2. MATERIALS AND METHODS

2.1 AlSi10Mg powder

AlSi10Mg is one of the widely used aluminium alloys in the metal AM industry, having low density and excellent weldability. AlSi10Mg components can be manufactured by L-PBF with low shrinkage, good dimensional accuracy, and high thermal conductivity [15, 16].

The AlSi10Mg powder used in this study was commercially available and sourced from Carpenter Additive® (Carpenter Additive (UK) Ltd, Widnes, UK). The nominal chemical composition with each element's boiling temperature and weight percentage are listed in Table 1.

The main aim of this study was to control the chemical composition to a targeted value using the potential preferential evaporation effect. Magnesium was selected as the target element, as it has significantly lower boiling temperature compared with the other elements, especially lower than the main elements aluminium and silicon. Magnesium also has sufficient wt.% in the AlSi10Mg alloy to be able to detect, adjust and trace. Zinc has lower boiling temperature than magnesium, but its potential wt.% adjusting range is insufficient for this study.

The initial Mg content of the AlSi10Mg powder was measured using Energy-dispersive X-ray spectroscopy (EDX) analysis (Hitachi TM3030Plus Tabletop Microscope) and was found to be 0.44±0.01 wt.%, which is at the upper end of the nominal composition (Table 1).

Table 1. Chemical composition of AlSi10Mg and each element's boiling temperature [17-19]

Element	Boiling Temperature (°C)	Nominal Chemical Composition (wt.%)	Measured Chemical Composition (wt.%)
Al	2470	Balance	89.67±0.04
Si	3265	9.00-11.00	9.75±0.03
Mg	1090	0.20-0.45	0.44±0.01
Zn	907	0.10	-
Pb	1749	0.05	-
Mn	2061	0.45	-
Cu	2562	0.05	-
Sn	2602	0.05	-
Ni	2730	0.05	-
Fe	2861	0.55	0.14±0.03
Ti	3287	0.15	-

2.2 Fabrication parameters

It is likely that the selective evaporation effect in the L-PBF of metal alloys is linked to the maximum temperature inside the melting pool and the total exposure time near the maximum temperature [5]. Laser energy density (LED), controlled by laser scanning parameters, determines the melting pool temperature in the L-PBF process. Therefore, a series of laser scanning parameters were developed to control the weight percentage of Mg in the fabricated samples. Main laser scanning parameters – laser power, scanning speed and hatch distance were adjusted, grouped, and listed in Table 2. LED for each parameter set was calculated and listed in Table 2. The parameters used in this study were extended out of the optimised process window, with the highest energy density 377.55 J/cm^2 was more than 4 times the lowest energy density 84.67 J/cm^2. This design of experiments (DOE) was developed to achieve a wide range in wt.% of Mg in the final samples. Also, the parameter sets were devised to assess the effect of maintaining two parameters constant and effecting an energy density change by varying the rest one parameter, thus investigating the effect on the Mg level, if any, of 'how' the energy density was delivered. The layer thickness was set constantly at 30 μm. Each parameter set was repeated once in the same build.

Solid cylinders 30 mm in diameter and 20 mm in height were manufactured by EOS EOSINT M 280 metal 3D printer. The size and the shape of the samples allow easy polishing and chemical composition measurement. The samples were built directly on the building platform with no support structures. After the build, the samples were removed from the building platform by

Wire-cut Electrical discharge machining (EDM) (Excetek V650G). No heat treatment nor any other post processes were performed.

Table 2. Process parameters used for fabricating AlSi10Mg samples, grouped by laser scanning parameters adjusting methods

Variability	Hatch distance (mm)	Scanning speed (mm/s)	Laser power (W)	LED (J/cm^2)
Hatch distance	0.14	1300	370	203.30
	0.19	1300	370	149.80
	0.24	1300	370	118.59
Laser powers	0.19	1300	330	133.60
	0.19	1300	350	141.70
	0.19	1300	370	149.80
Scanning speed, hatch distance 0.14mm	0.14	700	370	377.55
	0.14	800	370	330.36
	0.14	900	370	293.65
	0.14	1100	370	240.26
	0.14	1300	370	203.30
Scanning speed, hatch distance 0.19mm	0.19	900	370	216.37
	0.19	1100	370	177.03
	0.19	1300	370	149.80
	0.19	1500	370	129.82
	0.19	1700	370	114.55
	0.19	1900	370	102.49
	0.19	2100	370	92.73
	0.19	2300	370	84.67

2.3 Chemical composition measurement

Optical Emission Spectroscopy (OES) analysis (Oxford Instruments Foundry-master Pro) was used to measure the chemical composition in the fabricated cylinders. Each sample was polished using P400 sandpaper to achieve a flat surface, then measured 6 times, resulting in total 12 measurements for each laser scanning parameter set. The 6 measurement positions on each sample were kept the same for all the cylinders.

2.4 Properties examination

Each cylinder sample was polished in 4 steps (P400 CarbiMet, 9 μm TexMet, 3 μm TriDent, and final stage ChemoMet) using Buehler AutoMet 300 grinder-polisher to achieve a flat and scratch-free surface, and then examined under Nikon Eclipse LV150N optical microscope to check the porosity level. Tensile test specimens designed following ASTM E8 [20] were built using the same laser scanning parameter sets in Table 2 and pulled by static tension tests at 1 mm/min using Instron Testing System with 30KN static load cell. These specimens were built in upright position, with the overall length in Z build direction; and were built directly on the building platform with no support structures. 6 tensile specimens were built and tested for each laser scanning parameter set. After the build, the samples were removed from the building platform by Wire-cut Electrical discharge machining (EDM) (Excetek V650G). No heat treatment nor any other post processes were performed.

3. RESULTS AND DISCUSSION

3.1 Chemical composition change

Figure 1 shows the weight percentage of Mg in the fabricated samples under each set of main adjusted laser scanning parameters.

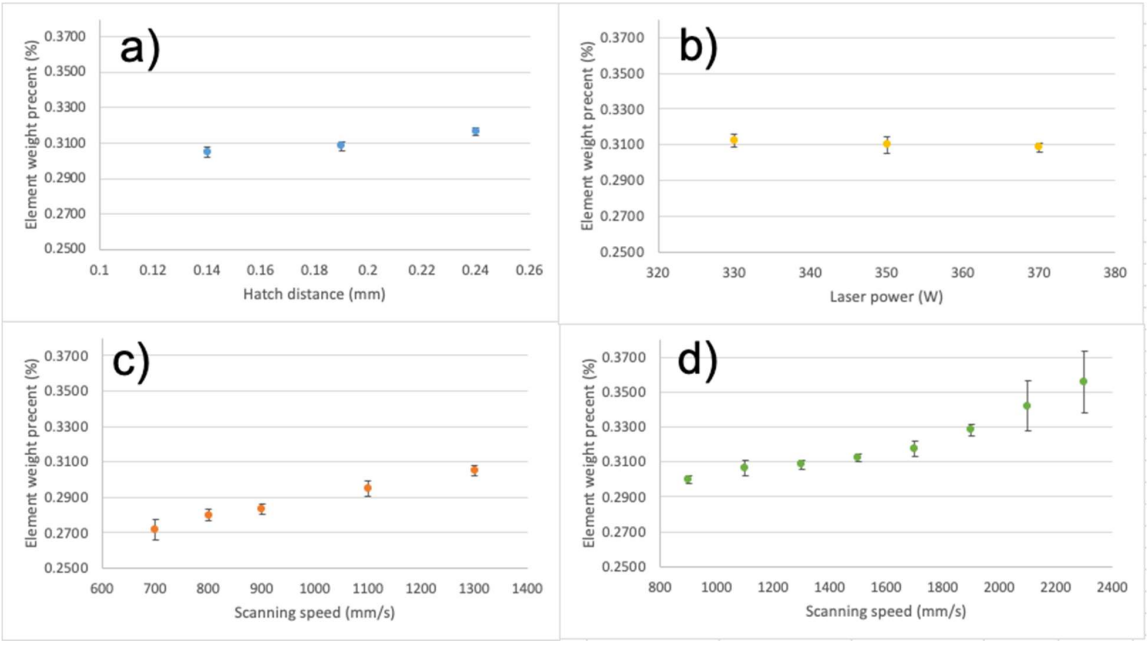

Figure 1. Weight percentage of Mg in fabricated cylinder samples: a) various hatch distance; b) various laser power; c) various laser scanning speed at 0.14 mm hatch distance; d) various laser scanning speed at 0.19 mm hatch distance

When the hatch distance increased from 0.14 mm to 0.24 mm (Figure 1a), the loss of Mg was slightly reduced. With the distance between successive laser passes increased, the width of the melting pool is expected to have decreased [21], leading to a shorter exposure time near the maximum temperature in the heat affected zone (HAZ) for the consolidated part.

With the laser power increased from 330 W to 370 W (Figure 1b), there was more energy delivered to the powder bed, resulting in higher melting pool temperature. This led to slightly more loss of Mg in the fabricated samples.

Laser scanning speed changes varied the weight percentage of Mg in the fabricated samples significantly. When the hatch distance was 0.14 mm (Figure 1c), a slow scanning speed at 700 mm/s resulted in the maximum loss of Mg in this study; while fast scanning speed at 2,300 mm/s, combined with a larger hatch distance 0.19mm (Figure 1d) resulted in the minimum loss of Mg. Adjusting laser scanning speed changed the laser energy density, as well as the exposure time of the maximum temperature from the melting pool.

Based on these results, it is likely that the evaporation of Mg could be linked to both the maximum temperature reached in the melting pool, and the total exposure time near the maximum temperature in the heat affected zone. The same effect was previously observed in titanium and nickel alloys [5, 14].

Figure 2. shows the weight percentage of Mg in the fabricated cylinders under different laser energy densities.

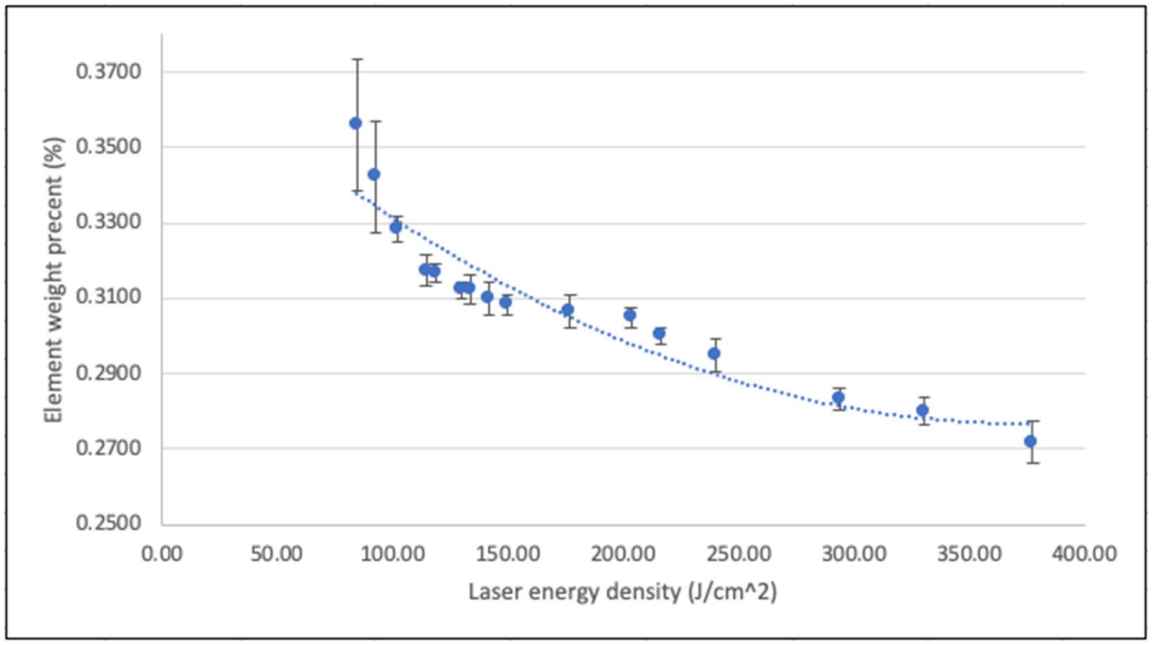

Figure 2. Weight percentage of Mg in the fabricated samples built by different laser energy densities

There is a clear link between the loss of Mg and LED. When the LED increased, the loss of Mg increased as well. The minimum loss of Mg happened at an LED of 84.67 J/cm^2, when the weight percentage of Mg decreased from 0.440 % to 0.356 %; and the maximum loss of Mg happened at an LED of 377.55 J/cm^2, when the weight percentage of Mg dropped down to 0.272%. The difference between the maximum and minimum weight percentage of Mg reached 0.084% in this study. With even wider range of LED values used, the changes of the chemical composition might show a larger difference; but the parts would be manufactured by the parameters further away from the optimised process window, and the quality could not be guaranteed.

3.2 Parts' quality examination

Since the laser process parameters used in this study were extended out of the optimised process window, it was necessary to assess the quality of the samples, especially the ones manufactured using the extreme LEDs.

Figure 3. shows the cross-section images taken from the optical microscopic analysis for the samples made under different LED. The highest density of the parts was achieved when using laser energy density 203.3 J/cm^2; while although the minimum and maximum LED used in this study produced traceable difference in chemical composition, the porosity levels in the parts were high.

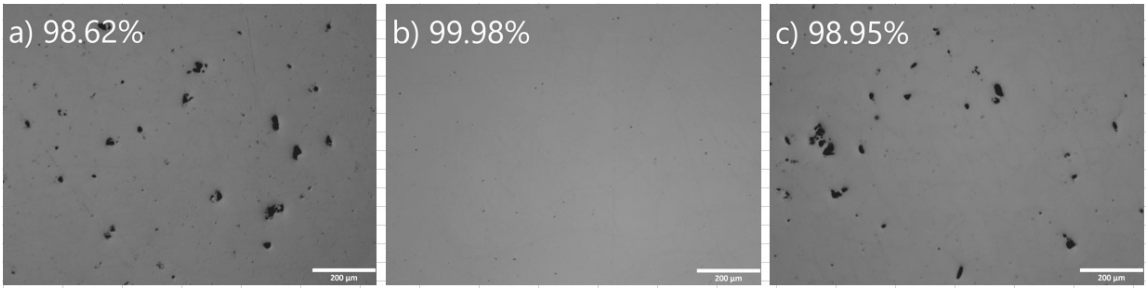

Figure 3. Cross section images of fabricated cylinder samples showing porosity level: a) minimum laser energy density 84.67 J/cm^2; b) laser energy density 203.3 J/cm^2; c) maximum laser energy density 377.55 J/cm^2

Figure 4. shows the Ultimate Tensile Strength (UTS) values of tensile test specimens built under each main adjusted LEDs as secondary axis data series added to the wt.% of Mg graphs. In contrast to the linear trend observed for Mg loss (Figure 1), the tensile properties changed significantly when the LEDs used were inside or outside the optimised process window. Each main LED – hatch distance, laser power, scanning speed, affects the tensile strength differently.

Figure 5. shows the UTS values under the weight percentage of Mg achieved in this study. When the wt.% of Mg dropped to 0.306 %, tensile strength of the parts decreased significantly when the loss of Mg increased. To maintain the tensile strength above 90 % of the maximum value achieved in this study, which is around 290 MPa, the corresponding weight percentage of Mg range was 0.308 wt.% - 0.342 t.%. The difference in wt.% within this range was only 0.034 wt.% rather than the full range difference 0.084 wt.%. This result suggested that the components' quality would be sacrificed to achieve the traceable chemical composition changes in AlSi10Mg alloy.

Therefore, using the preferential evaporation method to control the chemical composition in AlSi10Mg after L-PBF process should only be applied to non-critical areas of the components.

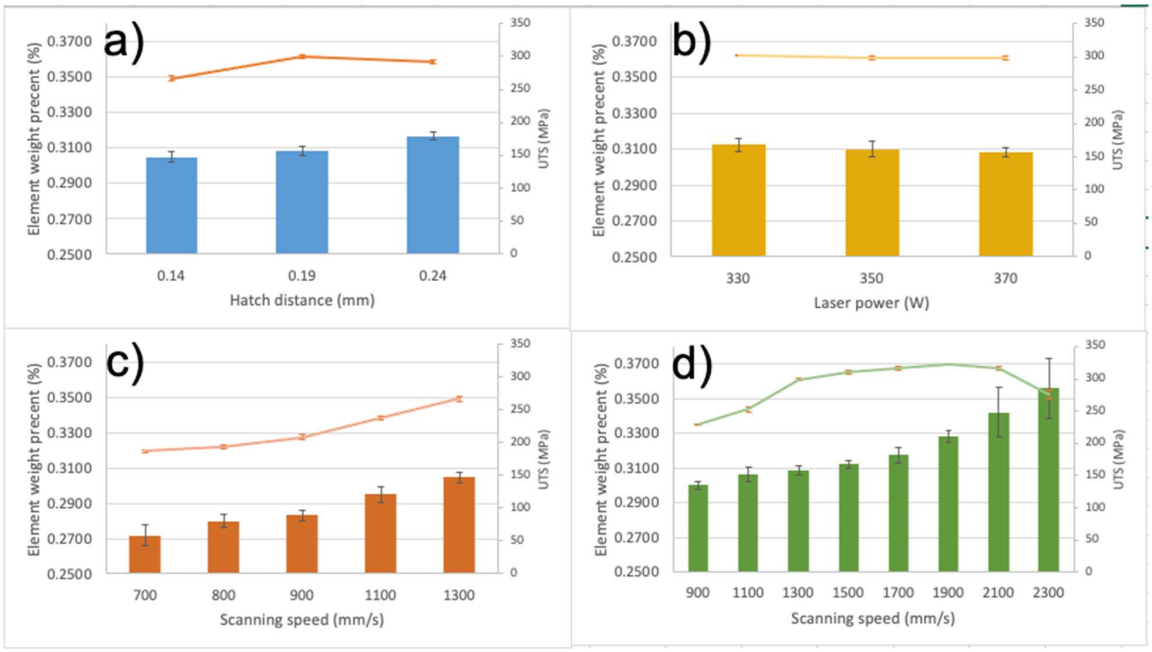

Figure 4. Ultimate Tensile Strength (solid lines) added to weight percentage of Mg (in clustered column) charts: a) various hatch distance; b) various laser power; c) various laser scanning speed at 0.14 mm hatch distance; d) various laser scanning speed at 0.19 mm hatch distance

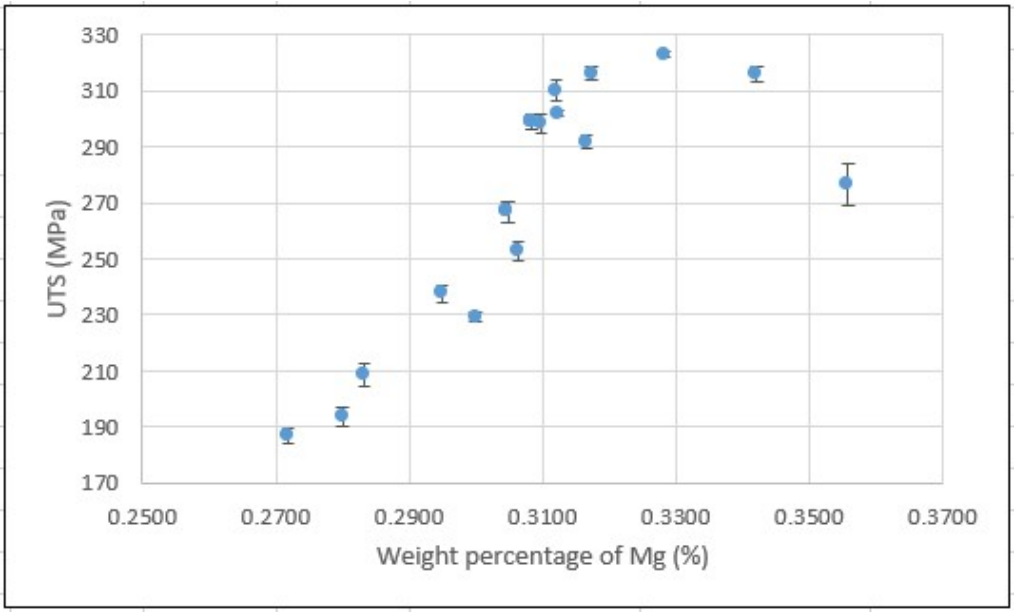

Figure 5. U Ultimate Tensile Strength against the weight percentage of Mg

4. CONCLUSION

Similar to titanium and nickel alloys, the selective evaporation effect was observed in AlSi10Mg alloy in this study. The main degrading element was magnesium.

By adjusting the main laser scanning parameters to achieve various laser energy density, the loss of Mg in the fabricated parts can be controlled. A total difference of 0.084% in weight percentage of Mg was achieved in this study.

The process parameters used to achieve the maximum and minimum loss of Mg were outside of the optimised process window, leading to the reduced parts' properties. To achieve traceable loss of Mg using the preferential evaporation effect, quality sacrifice needs to be considered in the product design and application.

5. ACKNOWLEDGEMENTS

This work was supported by the Engineering and Physical Sciences Research Council (EPSRC), UK [EP/V051040/1]

6. REFERENCES

[1] Gibson I, Rosen D, Stucker B, Khorasani M. Additive Manufacturing Technologies. 3rd ed. New York: Springer, Cham; 2021.

[2] W. E. King, A. T. Anderson, R. M. Ferencz, N. E. Hodge, C. Kamath, S. A. Khairallah, A. M. Rubenchik; Laser powder bed fusion additive manufacturing of metals; physics, computational, and materials challenges. Applied Physics Reviews 1 December 2015; 2 (4): 041304.

[3] Walaa Abd-Elaziem, Sally Elkatatny, Abd-Elrahim Abd-Elaziem, Mahmoud Khedr, Marwa A. Abd El-baky, Mohamed Ali Hassan, Mohamed Abu-Okail, Moustafa Mohammed, Antti Järvenpää, Tarek Allam, Atef Hamada, On the current research progress of metallic materials fabricated by laser powder bed fusion process: a review, Journal of Materials Research and Technology, Volume 20, 2022, Pages 681-707, ISSN 2238-7854.

[4] X. Cao, M. Jahazi, J.P. Immarigeon, W. Wallace, A review of laser welding techniques for magnesium alloys, Journal of Materials Processing Technology, Volume 171, Issue 2, 2006, Pages 188-204, ISSN 0924-0136.

[5] J.P. Oliveira, A.D. LaLonde, J. Ma, Processing parameters in laser powder bed fusion metal additive manufacturing, Materials & Design, Volume 193, 2020, 108762, ISSN 0264-1275.

[6] Xuezhi Shi, Shuyuan Ma, Changmeng Liu, Qianru Wu, Parameter optimization for Ti-47Al-2Cr-2Nb in selective laser melting based on geometric characteristics of single scan tracks, Optics & Laser Technology, Volume 90, 2017, Pages 71-79, ISSN 0030-3992.

[7] Alexander Klassen, Vera E. Forster, Vera Juechter, Carolin Körner, Numerical simulation of multi-component evaporation during selective electron beam melting of TiAl, Journal of Materials Processing Technology, Volume 247, 2017, Pages 280-288, ISSN 0924-0136.

[8] Wayne E. King, Holly D. Barth, Victor M. Castillo, Gilbert F. Gallegos, John W. Gibbs, Douglas E. Hahn, Chandrika Kamath, Alexander M. Rubenchik, Observation of keyhole-mode laser melting in laser powder-bed fusion additive manufacturing, Journal of Materials Processing Technology, Volume 214, Issue 12, 2014, Pages 2915-2925, ISSN 0924-0136.

[9] Ross Cunningham et al., Keyhole threshold and morphology in laser melting revealed by ultrahigh-speed x-ray imaging. Science 363, 849-852 (2019). DOI: 10.1126/science.aav4687

[10] Jan Schwerdtfeger, Carolin Körner, Selective electron beam melting of Ti–48Al–2Nb–2Cr: Microstructure and aluminium loss, Intermetallics, Volume 49, 2014, Pages 29-35, ISSN 0966-9795.

[11] Murr L. E., Gaytan S. M., Medina F., Lopez H., Martinez E., Machado B. I., Hernandez D. H., Martinez L., Lopez M. I., Wicker R. B. and Bracke J. 2010Next-generation biomedical implants using additive manufacturing of complex, cellular and functional mesh arraysPhil. Trans. R. Soc. A.3681999–2032.

[12] V. Juechter, T. Scharowsky, R.F. Singer, C. Körner, Processing window and evaporation phenomena for Ti–6Al–4V produced by selective electron beam melting, Acta Materialia, Volume 76, 2014, Pages 252-258, ISSN 1359-6454.

[13] Nandwana, P., Peter, W.H., Dehoff, R.R. et al. Recyclability Study on Inconel 718 and Ti-6Al-4V Powders for Use in Electron Beam Melting. Metall Mater Trans B 47, 754–762 (2016).

[14] Ma J., Franco B., Tapia G., Karayagiz K., Johnson L., Liu J., Arroyave R., Karaman I., Elwany A. Spatial control of functional response in 4D-printed active metallic structures. (2017) Scientific Reports, 7, art. no. 46707, 2017.

[15] Takahiro Kimura, Takayuki Nakamoto, Tomoatsu Ozaki, Kazuki Sugita, Masataka Mizuno, Hideki Araki, Microstructural formation and characterization mechanisms of selective laser melted Al–Si–Mg alloys with increasing magnesium content, Materials Science and Engineering: A, Volume 754, 2019, Pages 786-798, ISSN 0921-5093.

[16] Guo, Y., Han, Q., Hu, J. et al. Comparative Study on Wire-Arc Additive Manufacturing and Conventional Casting of Al–Si Alloys: Porosity, Microstructure and Mechanical Property. Acta Metall. Sin. (Engl. Lett.) 35, 475–485 (2022).

[17] Carpenter Additive® PowderRange AlSi10Mg Datasheet: https://www.carpenteradditive.com/hubfs/Resources/Data%20Sheets/PowderRange_AlSi10Mg_DataSheet.pdf

[18] Haynes, William M., ed. (2011). CRC Handbook of Chemistry and Physics (92nd ed.). CRC Press. ISBN 978-1439855119.

[19] Zhang Y; Evans JRG and Zhang S (2011). "Corrected Values for Boiling Points and Enthalpies of Vaporization of Elements in Handbooks". J. Chem. Eng. Data. 56 (2): 328–337. doi:10.1021/je1011086

[20] ASTM International. ASTM E8/E8M standard test methods for tension testing of metallic materials. West Conshohocken, PA 19428-2959 USA 2013.

[21] Dong Z, Liu Y, Wen W, Ge J, Liang J. Effect of Hatch Spacing on Melt Pool and As-built Quality During Selective Laser Melting of Stainless Steel: Modeling and Experimental Approaches. Materials (Basel). 2018 Dec 24;12(1):50. doi: 10.3390/ma12010050. PMID: 30586893; PMCID: PMC6337478.